Available online at www.sciencedirect.com
ScienceDirect
Journal of Sound and Vibration 312 (2008) 74–93
JOURNAL OF SOUND AND VIBRATION
www.elsevier.com/locate/jsvi

Localization of short-range acoustic and seismic wideband sources: Algorithms and experiments

J.Z. Stafsudd[a], S. Asgari[a], R. Hudson[a], K. Yao[a], E. Taciroglu[b,*]

[a]*Electrical Engineering Department, University of California, Los Angeles, CA 90095, USA*
[b]*Civil & Environmental Engineering Department, University of California, Los Angeles, CA 90095, USA*

Received 4 April 2006; received in revised form 5 June 2006; accepted 16 October 2007
Available online 3 December 2007

Abstract

We consider the determination of the location (source localization) of a disturbance source which emits acoustic and/or seismic signals. We devise an enhanced approximate maximum-likelihood (AML) algorithm to process data collected at acoustic sensors (microphones) belonging to an array of, non-collocated but otherwise identical, sensors. The approximate maximum-likelihood algorithm exploits the time-delay-of-arrival of acoustic signals at different sensors, and yields the source location. For processing the seismic signals, we investigate two distinct algorithms, both of which process data collected at a single measurement station comprising a triaxial accelerometer, to determine direction-of-arrival. The direction-of-arrivals determined at each sensor station are then combined using a weighted least-squares approach for source localization. The first of the direction-of-arrival estimation algorithms is based on the spectral decomposition of the covariance matrix, while the second is based on surface wave analysis. Both of the seismic source localization algorithms have their roots in seismology; and covariance matrix analysis had been successfully employed in applications where the source and the sensors (array) are typically separated by planetary distances (i.e., hundreds to thousands of kilometers). Here, we focus on very-short distances (e.g., less than one hundred meters) instead, with an outlook to applications in multi-modal surveillance, including target detection, tracking, and zone intrusion. We demonstrate the utility of the aforementioned algorithms through a series of open-field tests wherein we successfully localize wideband acoustic and/or seismic sources. We also investigate a basic strategy for fusion of results yielded by acoustic and seismic arrays.

1. Introduction

Distributed sensor networks have been utilized in a wide range of applications; and herein, we consider surveillance applications. The main purpose of a surveillance sensor network is to monitor an area by detecting, localizing, tracking, and classifying (DLTC) one or more objects of interest. Such systems are needed for safeguarding the perimeter and environs of critical structures (e.g., power plants, dams, major highway crossings), lifelines (e.g., electric, gas, oil transmission lines), and national borders.

In this study, our goal is to detect and to localize (i.e., determine the position of) a near-field source, generating acoustic and/or seismic wideband signals. Examples of sources possessing the aforementioned

*Corresponding author. Tel.: +1 310 2674655.
E-mail address: etacir@ucla.edu (E. Taciroglu).

0022-460X/$ - see front matter © 2007 Elsevier Ltd. All rights reserved.
doi:10.1016/j.jsv.2007.10.040

attributes are on-foot intruders and terrestrial vehicles. Under normal circumstances, acoustic and seismic signals from such sources are not detectable over large distances due to their relatively small energy output, and the geometric and hysteretic (due to material damping) attenuation of this energy within the propagation medium. At the present time, advances in this particular area are limited, primarily due to lack of experimental data that help improve and validate feasible methods for detecting, localizing, tracking, and classifying [1].

In order to aid our method development efforts and to validate and to assess the performance of the developed methods, we utilize data collected during a series of open-field tests. The setup of these tests consisted of two acoustic arrays (each comprising four closely spaced, omnidirectional, low-cost microphones), and six triaxial state-of-the-art accelerometers. The sensors were placed on the ground with a typical separation of 15 m, and several scenarios were simulated, such as intrusion by vehicles, on-foot personnel, and medium-intensity impacts on the ground. The acoustic and seismic signals were recorded and time-synchronized with wireless data acquisition systems. For the present study, we shall only consider the impact sources, to focus the development efforts for detection and localization of stationary and very wideband sources.

For acoustic source localization, we start from an existing method, dubbed approximate maximum-likelihood (AML), originally developed for narrowband and relatively wideband sources [2]. Detailed chronicles of the applications of this method, and of the related/competing methods may be found in Refs. [2–4,11]. Henceforth referred to as the *original* approximate maximum likelihood, this method yields the direction-of-arrival (DOA) of the source signal in the coordinate system of the sensor array. If the direction-of-arrival data is available from at least two sensor arrays, they can be combined to yield the source location. Through the use of experimental data, we demonstrate that the original approximate maximum likelihood method's accuracy is unsatisfactory (with absolute errors in comparable magnitude to sensor array separation distances) for very wideband sources. We then present two enhancements to the original approximate maximum likelihood method that significantly improve the accuracy of estimations (with absolute estimation errors that are approximately 1 m).

For a seismic source, we use data collected at a single triaxial accelerometer to perform direction-of-arrival estimation. We consider two seismic direction-of-arrival estimation methods. The first method, dubbed covariance matrix analysis (CMA), is well-developed and has been utilized in long-range and/or high-energy seismic signal processing [5,6,8,9]. Applications of covariance matrix analysis include processing signals from tectonic events (i.e., when the sensor and the source are hundreds to thousands of kilometers apart) and in oil exploration (i.e., when the seismic signal is generated by high-energy explosions). Using short-range, low-energy field test data, we compare the performance of covariance matrix analysis to a method we develop here, named surface wave analysis (SWA), which is formulated under the assumption that the source is nearby, and polarized surface waves dominate the seismic signal.

In what follows, we first provide the details of the original approximate maximum likelihood algorithm and its necessary enhancements for determination of wideband acoustic source direction-of-arrival in Section 2, and of the two aforementioned methods for seismic source direction-of-arrival determination in Section 3. We then present a simple method for event detection in Section 4 that applies to both acoustic and seismic signals; and subsequently describe a weighted least-squares procedure for source localization using direction-of-arrival estimations in Section 5. These algorithmic developments are followed by Section 6 where we describe the field tests, and provide the results yielded by the acoustic and seismic source detection and localization algorithms. Conclusions is presented in Section 7, and finally acknowledgments is given.

2. AML algorithm for acoustic array direction-of-arrival estimation

As illustrated in Fig. 1, we assume that the sensor array comprises P randomly distributed, omnidirectional sensors with identical behavior. Each sensor is located at (known) position $\mathbf{r}_p = [x_p, y_p]^{\mathrm{T}}$ with $1 \leqslant p \leqslant P$; therefore, the array centroid position is given by

$$\mathbf{r}_c = \frac{1}{P}\sum_{p=1}^{P} \mathbf{r}_p = [x_c, y_c]^{\mathrm{T}}. \tag{1}$$

Similarly, we assume that there is a wideband source at the unknown location $\mathbf{q} = [X, Y]^{\mathrm{T}}$.

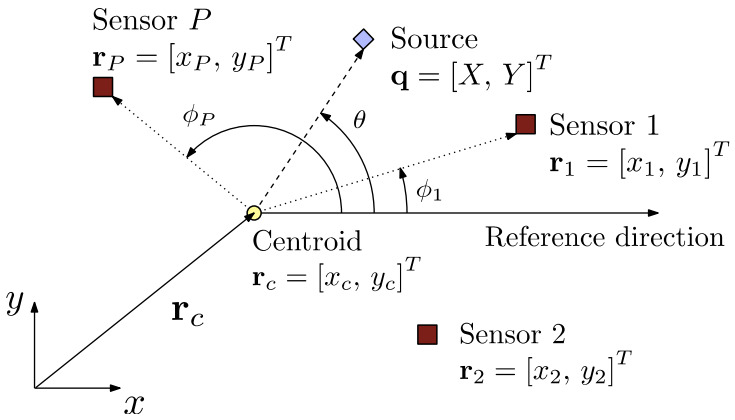

Fig. 1. Sensor and source geometry for the acoustic problem.

Upon creating a reference coordinate system at the array centroid with axes parallel to x and y, the range r_p, and the angle ϕ_p of the pth sensor with respect to the array centroid are given by

$$r_p = \|\mathbf{r}_p - \mathbf{r}_c\|, \quad \tan\phi_p = \frac{x_p - x_c}{y_p - y_c}. \tag{2}$$

Similarly, the (unknown) range q, and the angle θ of the source relative to the coordinate system at the array centroid can be calculated through

$$q = \|\mathbf{q} - \mathbf{r}_c\|, \quad \tan\theta = \frac{X - x_c}{Y - y_c}. \tag{3}$$

We use the array centroid as the reference point and define a signal model based on the relative time delays from this position. To wit, the relative time delay of the signal source is given by

$$t_{cp} = t_c - t_p = [(x_c - x_p)\cos\theta + (y_c - y_p)\sin\theta]/v, \tag{4}$$

where t_c and t_p are the absolute time delays from the signal source to the centroid and to the pth sensor, respectively; and v is the speed of propagation. In a polar coordinate system, the above relative time delay can also be expressed as

$$t_{cp} = r_p\cos(\theta - \phi_p)/v. \tag{5}$$

We note here that—given the known sensor locations and propagation speed—the relative time delay of the source is an explicit function of the bearing (azimuth) angle, i.e. $t_{cp} = t_{cp}(\theta)$. It follows that the data received by the pth sensor at time $t = t_n$ (henceforth, simply denoted by the index n) is given by

$$s_p(n) = s_0(n - t_{cp}) + z_p(n), \quad n = 0, \ldots, N-1, \tag{6}$$

where N is the length of the data vector, s_0 is the source signal at the array centroid position $\mathbf{r}_c$, and z_p is the zero-mean white Gaussian noise with variance σ^2.

For the ease of derivation and analysis, the received wideband signal can be transformed into the frequency domain via discrete Fourier transform (DFT), where a narrowband model can be attributed to each frequency bin.[1] By using an N-point discrete Fourier transform transformation (while omitting the unimportant zero frequency bin and the negative frequency bins that are merely mirror images of the positive frequency bins), the array data model in the frequency domain is given by

$$\mathbf{S}(k) = S_0(k)\mathbf{D}(k) + \boldsymbol{\eta}(k), \quad k = 1, \ldots, N/2, \tag{7}$$

[1]It is well-known that the circular shift property of the discrete Fourier transform has an edge effect problem for the actual linear time shift. These finite effects become negligible for sufficiently long data. Here, we assume the data length N is large enough to ignore the artifact caused by the finite data length [2].

where the index k denotes the discrete (positive) frequencies, say ω_k. In Eq. (7), the scalar $S_0(k)$ is the source spectrum, $\mathbf{S}(k) = [S_1(k), \ldots, S_P(k)]^{\mathrm{T}}$ is the (measured) array data spectrum vector, $\mathbf{D}(k) = [D_1(k), \ldots, D_P(k)]^{\mathrm{T}}$ is the steering vector with $D_p = \mathrm{e}^{-j2\pi k t_{cp}/N}$, and finally $\boldsymbol{\eta}(k) = [\eta_1(k), \ldots, \eta_P(k)]^{\mathrm{T}}$ is the complex white noise spectrum vector with a zero-mean Gaussian distribution[2] and variance $N\sigma^2$. Note that, although not explicitly stated in Eq. (7), the steering vector is a function of the unknown bearing angle, i.e., $\mathbf{D}(k) = \mathbf{D}(\theta, k)$.

The probability distribution of the complex Gaussian noise vector $\boldsymbol{\eta}$ over all the frequencies is given by

$$\mathscr{P}(\boldsymbol{\eta}) = \prod_{k=1}^{N/2}\prod_{p=1}^{P}\frac{1}{\sigma\sqrt{2\pi}}\,\mathrm{e}^{-\eta_p^2(k)/2\sigma^2} = \prod_{k=1}^{N/2}\prod_{p=1}^{P}\frac{1}{\sigma\sqrt{2\pi}}\mathrm{e}^{-(S_p(k)-S_0(k)D_p(k))^2/2\sigma^2}. \tag{8}$$

Thus, the log-likelihood function of the noise vector is

$$\begin{aligned}\log(\mathscr{P}(\boldsymbol{\eta})) &= \sum_{k=1}^{N/2}\sum_{p=1}^{P}\left[\log(1/\sigma\sqrt{2\pi}) - \frac{1}{2\sigma^2}(S_p(k) - S_0(k)D_p(k))^2\right] \\ &= \frac{NP}{2}\log(1/\sigma\sqrt{2\pi}) - \frac{1}{2\sigma^2}\sum_{k=1}^{N/2}\|\mathbf{S}(k) - S_0(k)\mathbf{D}(k)\|^2. \end{aligned} \tag{9}$$

After ignoring the irrelevant constant terms, the approximated maximum-likelihood of the source direction-of-arrival and the source signals is given by

$$\begin{aligned}\max_{\boldsymbol{\Theta}} L(\boldsymbol{\Theta}) &= \max_{\boldsymbol{\Theta}}\left[-\sum_{k=1}^{N/2}\|\mathbf{S}(k) - S_0(k)\mathbf{D}(k)\|^2\right] \\ &= \min_{\boldsymbol{\Theta}}\sum_{k=1}^{N/2}\|\mathbf{S}(k) - S_0(k)\mathbf{D}(k)\|^2, \end{aligned} \tag{10}$$

where $\boldsymbol{\Theta} \equiv [\theta, S_0(1), \ldots, S_0(N/2)]^{\mathrm{T}}$. This is equivalent to finding

$$\min_{[\theta, S_0(k)]} f(k) = \min_{[\theta, S_0(k)]}\|\mathbf{S}(k) - S_0(k)\mathbf{D}(k)\|^2 \tag{11}$$

for all k bins. Noting that the minima of $f(k)$ with respect to the source signal spectrum $S_0(k)$ must satisfy the first-order optimality condition, $\partial f(k)/\partial S_0(k) = 0$, the estimate of the source signal spectrum, say $S_0^*(k)$, that yields the minimum residual at the source location is given by

$$S_0^*(k) = [\mathbf{D}^H(k)\mathbf{D}(k)]^{-1}\mathbf{D}^H(k)\mathbf{S}(k) = \mathbf{D}^{\dagger}(k)\mathbf{S}(k), \tag{12}$$

where the superscript H denotes the complex conjugate transpose operation. Upon defining the orthogonal projection $\mathbf{P}(\theta, k) = \mathbf{D}(k)\mathbf{D}^{\dagger}(k)$, the complementary orthogonal projection becomes $\mathbf{P}^{\perp}(\theta, k) = \mathbf{I} - \mathbf{P}(\theta, k)$, where $\mathbf{I}$ is a $(P \times P)$ identity matrix. By substituting Eq. (12) into Eq. (11), the minimization function becomes

$$f(k) = \|\mathbf{P}^{\perp}(\theta, k)\mathbf{S}(k)\|^2. \tag{13}$$

After substituting the estimate of the source signal $S_0^*(k)$ in Eq. (12), the approximate maximum likelihood estimate of the source bearing angle θ can be obtained by solving

$$\begin{aligned}\max_{\theta} J(\theta) &= \min_{\theta}\sum_{k=1}^{N/2}\|\mathbf{P}^{\perp}(\theta, k)\mathbf{S}(k)\|^2 = \max_{\theta}\sum_{k=1}^{N/2}\|\mathbf{P}(\theta, k)\mathbf{S}(k)\|^2 \\ &= \max_{\theta}\sum_{k=1}^{N/2}\mathrm{tr}(\mathbf{P}(\theta, k)\mathbf{R}(k)), \end{aligned} \tag{14}$$

[2]Due to the transformation to the frequency domain, $\boldsymbol{\eta}(k)$ asymptotically approaches a Gaussian distribution by the central limit theorem even if the actual noise is arbitrary, independent and identically-distributed (with bounded variance) in the time domain. This asymptotic property in the frequency domain provides a more reliable noise model than the time domain model in some practical cases [2].

where $\mathbf{R}(k) = \mathbf{S}(k)\mathbf{S}^H(k)$ is the one snap-shot covariance matrix. After determining θ, the source signal estimate can be easily obtained through Eq. (12).

The presented AML algorithm estimates the source direction-of-arrival by maximizing the signal-to-noise-ratio (SNR) in a maximum-likelihood sense. The algorithm has been demonstrated to work very well for narrowband and relatively wideband sources (e.g., tracked vehicles, music-type sources, bird calls [12]). However, it has to be modified for a very wideband source. The modifications we describe in the following subsections are aimed at reducing the computational cost and increasing the signal power for approximate maximum likelihood estimation—both of which become critical issues when dealing with wideband signals. The utility of these modifications are subsequently demonstrated through the use of experimental data in Section 6.

2.1. Channel whitening

One of the important assumptions utilized in the development of the approximate maximum likelihood algorithm is that of uniformity of the noise spectral density in all of the channels. However, the background noise is generally non-uniform in the real world. When processing a wideband signal, the noise is also sampled at a broader frequency range, weakening this assumption. Therefore, a better model of background noise is necessary. Here, we opt to use channel whitening to reduce the effect of this non-uniformity. To perform the whitening, we first record the background noise (i.e., when the signal from an event is not present) and use this data to estimate the average power spectral density (PSD) of the background noise for each microphone channel. We then use the average power spectral density values to normalize the data when an event signal is present. The resulting signal is corrupted by "white noise," and we use it for approximate maximum likelihood direction-of-arrival estimation instead of the original "raw" data. The mathematical details of the channel whitening procedure are as follows:

Let us denote the background noise recorded through the pth channel in the time domain as $\hat{z}_p(n)$, where $n = \{0, 1, \ldots, L-1\}$. We divide this signal into B segments with 50% overlap, say $\hat{z}_p^i(n_i)$, where $i = \{1, 2, \ldots, B\}$ and

$$(i-1) \times (L-1)/(B+1) \leqslant n_i \leqslant (i+1) \times (L-1)/(B+1), \tag{15}$$

where we note that the noise data should be truncated accordingly if its length is such that it cannot be divided exactly into B sections with 50% overlap. The overlap is necessary to obtain accurate estimates of the power spectral density of background noise, and 15–75% overlap values usually yield reasonable estimations. Therefore the particular value of 50% is somewhat arbitrary.

After windowing each segment with a Hamming window, and subsequently performing an N-point discrete Fourier transform over each channel's data, we get $\hat{\eta}_p^i(k)$ where k denotes the frequency ω_k as before (see, for example, Eq. (7). The average power spectral density of the background noise for each microphone channel is then

$$\varrho_p^{\mathrm{PSD}}(k) = \frac{1}{B}\sum_{i=1}^{\mathrm{B}} |\hat{\eta}_p^i(k)|^2. \tag{16}$$

Finally, we divide the complex-valued spectral amplitude (when signal is present) by the square root of the average noise power at each frequency and for each microphone channel. This yields the whitened version of the signal in the frequency domain. To wit,

$$\mathbf{S}_{\mathrm{white}}(k) = \left[\frac{S_1(k)}{\sqrt{\varrho_1^{\mathrm{PSD}}(k)}}, \frac{S_2(k)}{\sqrt{\varrho_2^{\mathrm{PSD}}(k)}}, \ldots, \frac{S_P(k)}{\sqrt{\varrho_P^{\mathrm{PSD}}(k)}}\right]. \tag{17}$$

2.2. Frequency-bin selection

The second difference between the present and the original maximum-likelihood estimation algorithm is the use of a better frequency bin selection process. This new process is primarily aimed at reducing

computational cost, but will also improve the accuracy of estimations through proper weighting of data. To wit, Eq. (14) shows that we have to add the trace of a matrix for $N/2$ different frequency bins in order to compute the maximum-likelihood criterion. When the source signal is wideband, with the appropriate sampling frequency, N may become a large number. Thus, the complexity of the approximate maximum likelihood algorithm becomes quite high. In order to reduce the complexity, we have to choose a small subset of $N/2$ frequency bins, and apply the approximate maximum likelihood algorithm to that subset. By a proper selection of this subset of frequency bins, we may be able to maintain the accuracy of approximate maximum likelihood estimation with all data, but now with a much reduced computational cost.

Let us define a weighted complex amplitude spectra, which is summed over all channels, as the following:

$$\varrho(k) = c_k \times \sum_{p=1}^{P} |S_p(k)|^2, \tag{18}$$

where, as before, $k \in A \equiv \{1, 2, \ldots, N/2\}$, and thus, A is the full set of frequencies. It is important to note that the sampling rate of typical acoustic sensors is in the kilo-Hertz range, and thus, processing all frequencies without discrimination will create a computational bottleneck and render real-time source localization very difficult, if not impossible, in realistic scenarios. Because it is reasonable to expect that the total spectral power, i.e.

$$P_A = \sum_{k \in A} \varrho(k) \tag{19}$$

is not uniformly distributed among the full set of frequencies (even for a wideband signal) we may choose only a subset of frequencies for approximate maximum likelihood processing in order to achieve computational efficiency. In order to choose this subset we first divide the vector $\boldsymbol{\varrho}$ into approximately L^2 sub-vectors as in

$$\boldsymbol{\varrho} = [\varrho(1), \varrho(2), \ldots, \varrho(N/2)] = [\mathbf{B}_1, \mathbf{B}_2, \ldots, \mathbf{B}_{L^2}], \tag{20}$$

where the length of each sub-vector (say $\mathbf{B}_m$) is equal to $(1/L) \times \text{ceil}(N/(2L))$. We then obtain the global maximum of each sub-vector as

$$B_m^{\max} \equiv \max(\mathbf{B}_m). \tag{21}$$

Finally, we choose the L largest of all $B_m^{\max}$ values, and define the subset of frequencies to be processed as those belonging to these L bins, and discard the rest. For the experimental data that will be presented in Section 6, we have used $N/2 = 2250$, and processed only $L = 25$ of these that satisfied the selection criterion outlined above (i.e., we have discarded nearly $1 - 25/2250 \cong 98.8\%$ of the frequency-domain data). Note that, this strategy allows the selection of representative frequencies from each bin, and thus, increases computational efficiency while reducing the possibility of frequencies scattered around a only a few peaks to dominate the subset.

Another important issue in subset selection is the choice of the weight factors. For wideband signals, more useful information is generally stored in the higher frequencies simply because they are sampled more frequently by the sensors. Furthermore, the background noise (e.g., wind noise) is more concentrated in the low frequencies. Therefore, we choose the weighting parameter in Eq. (18) as $c_k = \omega_k^2$ in order to give more weight to data received in the higher frequencies.

3. Seismic direction-of-arrival estimation with a single triaxial station

Signals from a generic seismic event contain primary and secondary (P and S) body waves, as well as surface (Rayleigh and Love) waves, with each type of wave exhibiting different frequency content and velocity from others. In this study, we shall focus on seismic events for which (i) the source and the sensor are separated by short distances (e.g., a few hundred meters or less), (ii) they both reside on the surface (or near the surface) of an elastic half-space, and (iii) the source emits a relatively weak signal (as compared to an earthquake) such as that by travelling or idling vehicles, footsteps, impact and collisions, and even small-yield detonations. Under these conditions, the Rayleigh and Love waves dominate the signal. Rayleigh wave exhibits a rolling motion in

the direction of propagation, occupying the vertical direction (the direction perpendicular to the ground) and the direction of propagation on the ground plane. Love wave produces side-to-side motion perpendicular to the direction of propagation on the ground plane. The earth acts as a frequency and velocity filter as the seismic signals propagate. Signals collected by long-range sensors exhibit separation of the P, S, Rayleigh and Love waves in the frequency domain as well as on the arrival time-line. Short-range seismic signals do not have the benefit of filtration, and hence the Rayleigh and Love waves arrive at approximately the same time, and are overlapped in the frequency domain.

In the following subsections we shall consider two alternative methods for determination of seismic direction-of-arrival using single triaxial station data. The first of these methods is based on the so-called covariance matrix analysis. This existing method [6] has been devised primarily for spectral analysis and localization of long-to-medium range, and strong-to-mild events (e.g., earthquakes, nuclear detonations, oil exploration, etc.). The second method, which we refer to as surface wave analysis, is novel and is specifically designed for localization of short-range, weak surface events. In what follows, we first provide the details of these two methods (covariance matrix analysis in Section 3.1, surface wave analysis in Section 3.2) and later compare their performance using data collected in a suite of field experiments (Section 6).

3.1. Seismic direction-of-arrival estimation via spectral decomposition of the covariance matrix

The covariance matrix analysis method for seismic direction-of-arrival estimation is based on the spectral decomposition of the signal covariance matrix [6,7]. We first reproduce its basic formulas here for the convenience of the reader, and subsequently discuss the use of covariance matrix analysis for seismic direction-of-arrival estimation.

Consider a time-sampled acceleration signal along x, y, and z directions, collected at a triaxial station and organized into $(N \times 1)$ signal vectors as

$$\begin{aligned}\mathbf{s}_x &= [s_x(N_o), s_x(N_o+1), \ldots, s_x(N_o+N-1)]^{\mathrm{T}},\\ \mathbf{s}_y &= [s_y(N_o), s_y(N_o+1), \ldots, s_y(N_o+N-1)]^{\mathrm{T}},\\ \mathbf{s}_z &= [s_z(N_o), s_z(N_o+1), \ldots, s_z(N_o+N-1)]^{\mathrm{T}},\end{aligned} \tag{22}$$

where the time indices N_o and N, respectively, denote the beginning and the extent of a time window, which contains an event of interest. A simple heuristic "event-detection" algorithm used for determining these indices is discussed later in Section 4. These vectors form the columns of the $(N \times 3)$ the signal matrix (for each window) given by

$$\mathbf{S} = [\mathbf{s}_x \;\; \mathbf{s}_y \;\; \mathbf{s}_z]. \tag{23}$$

Singular-value decomposition of the signal matrix yields

$$\mathbf{S} = \mathbf{U}\mathbf{W}\mathbf{V}^{\mathrm{T}}. \tag{24}$$

The matrices on the right-hand side of Eq. (24) are given by

$$\mathbf{U} = [\mathbf{u}^{(1)}, \mathbf{u}^{(2)}, \mathbf{u}^{(3)}], \quad \mathbf{W} = \mathrm{diag}[\lambda_1, \lambda_2, \lambda_3], \quad \mathbf{V} = [\mathbf{v}^{(1)}, \mathbf{v}^{(2)}, \mathbf{v}^{(3)}], \tag{25}$$

where scalars $\lambda_i, i \in \{1,2,3\}$ denote the square-root of the eigenvalues of the (3×3) inner product matrix $\mathbf{S}^{\mathrm{T}}\mathbf{S}$; or equivalently,[3] those of the $(N \times N)$ outer product matrix $\mathbf{S}\mathbf{S}^{\mathrm{T}}$. Here, we assume that the eigenvalues are ordered such that

$$\lambda_1 \leqslant \lambda_2 \leqslant \lambda_3. \tag{26}$$

Correspondingly, the $(N \times 1)$ vectors $\mathbf{u}_i$, and the (3×1) vectors $\mathbf{v}_i$, are the eigenvectors of the outer product $(\mathbf{S}\mathbf{S}^{\mathrm{T}})$, and the inner product $(\mathbf{S}^{\mathrm{T}}\mathbf{S})$ signal matrices, respectively. The inner product of the signal matrix is

[3]The outer product matrix $\mathbf{S}\mathbf{S}^{\mathrm{T}}$ is rank-deficient and its non-zero eigenvalues (of which it has three) are equal to the eigenvalues of $\mathbf{S}^{\mathrm{T}}\mathbf{S}$.

typically referred to as the *cross-energy matrix* or the *covariance matrix*, and can be explicitly stated as

$$\mathbf{M} = \mathbf{S}^{\mathrm{T}}\mathbf{S} = \sum_{n=N_o}^{N_o+N} \begin{pmatrix} s_x^2(n) & s_x(n)s_y(n) & s_x(n)s_z(n) \\ s_y(n)s_x(n) & s_y^2(n) & s_y(n)s_z(n) \\ s_z(n)s_x(n) & s_z(n)s_y(n) & s_z^2(n) \end{pmatrix}. \tag{27}$$

The spectral decomposition of the covariance matrix yields its eigenvalues and eigenvectors. To wit,

$$\mathbf{M} = \mathbf{S}^{\mathrm{T}}\mathbf{S} = \mathbf{V}\mathbf{W}\mathbf{U}^{\mathrm{T}}\mathbf{U}\mathbf{W}\mathbf{V}^{\mathrm{T}} = \mathbf{V}\mathbf{W}^2\mathbf{V}^{\mathrm{T}}. \tag{28}$$

Each eigenvalue (λ_i^2) corresponds to the average energy of the seismic mode polarized in the direction of its corresponding eigenvector, $\mathbf{v}^{(i)}$. For each eigenvector, an azimuth and a depression angle can be computed through

$$\alpha_i = \tan^{-1}(v_2^{(i)}/v_1^{(i)}), \quad \gamma_i = \tan^{-1}(v_3^{(i)}/\sqrt{v_1^{(i)}v_1^{(i)} + v_2^{(i)}v_2^{(i)}}). \tag{29}$$

The azimuth angle (α_i) is defined as the angle measured counter-clockwise from the x-axis on the ground (i.e., $z = 0$) plane, whereas the depression angle (γ_i) is defined as the downwards angle measured from ground plane.

Rayleigh wave is elliptically polarized and occupy two orthogonal directions. Love wave is rectilinearly polarized in the direction orthogonal to the direction of propagation. Therefore, if the Rayleigh wave dominates the energy of the received signal as compared to the Love wave, then the azimuth angle determined from components of $\mathbf{v}^{(3)}$ yields the direction-of-arrival estimate. On the other hand, if the Love wave dominates signal energy, the azimuth angle determined from components of $\mathbf{v}^{(3)}$ is *perpendicular* to the direction-of-arrival. There are two directions that are perpendicular to the particle motion for a Love wave so the computed azimuth angles have a 180° ambiguity. This ambiguity may be circumvented when direction-of-arrival estimates from multiple triaxial stations are available (see Section 5).

3.2. Seismic direction-of-arrival estimation via surface wave analysis

Let the vector $\mathbf{d}(t) = [d_x(t), d_y(t), d_z(t)]$ denote the displacement of a particle at a sensor location. Rayleigh wave exhibits an elliptical motion in the plane containing the vertical axis (z) and the direction of propagation (p), whereas Love wave exhibits a rectilinear motion along the direction, say q, perpendicular to the direction of propagation. Assuming that the direction of propagation lies solely in the ground ($z = 0$) plane (i.e., the depression angle is zero) and that this holds for the time interval $t \in [t_k, t_N]$, the following must be true

$$\frac{d_z^2(t)}{A^2} + \frac{d_p^2(t)}{B^2} = 1, \quad d_q(t) = C\eta(t), \quad \forall t \in [t_k, t_N], \tag{30}$$

where $d_p(t)$ and $d_q(t)$ denotes the particle displacements along p and q directions; $\eta(t)$ is a yet unknown function; and the coefficients A, B and C depend on the energy of the signal. If the time waveform of the ellipse in the p direction is

$$d_p(t) = B\sin(t), \tag{31}$$

then the time waveform of the ellipse in the z direction must be

$$d_z(t) = A\cos(t). \tag{32}$$

In other words, the signals in the z and p directions due to a Rayleigh wave are 90° out of phase. The particle displacements along the p and q directions are related to those along the x and y directions as

$$\begin{aligned} d_x(t) &= d_p(t)\cos(\alpha) - d_q(t)\sin(\alpha), \\ d_y(t) &= d_p(t)\sin(\alpha) + d_q(t)\cos(\alpha), \end{aligned} \tag{33}$$

where α denotes the azimuth angle of the direction of propagation and we have assumed that it remains constant within the time window $t \in [t_k, t_N]$. The accelerations along the x and y directions are then,

$$s_x(t) = \ddot{d}_x(t) = -d_p(t)\cos(\alpha) - C\ddot{\eta}(t)\sin(\alpha),$$
$$s_y(t) = \ddot{d}_y(t) = -d_p(t)\sin(\alpha) + C\ddot{\eta}(t)\cos(\alpha), \tag{34}$$

where the "double dots" denote the time derivative $\partial^2(\cdot)/\partial t^2$, and we have made use of the equivalency $\ddot{d}_p = -d_p$ (cf. Eq. (31)). Similarly, the velocity along the z direction is

$$v_z(t) = \dot{d}_z(t) = -A\sin(t) = -(A/B)d_p(t). \tag{35}$$

Therefore, except for the presence of the terms $\ddot{\eta}(t)$ in Eq. (34), this velocity signal is in-phase with, and proportional to the acceleration signals s_x, and s_y. The product of these terms yields

$$v_z(t) \times s_x(t) = (A/B)d_p^2(t)\cos(\alpha) - (AC/B)d_p(t)\ddot{\eta}(t)\sin(\alpha),$$
$$v_z(t) \times s_y(t) = (A/B)d_p^2(t)\sin(\alpha) + (AC/B)d_p(t)\ddot{\eta}(t)\cos(\alpha). \tag{36}$$

Here, we shall assume that the particle motion along p and q directions are uncorrelated. Consequently, if an average or an integral (over time) of Eq. (36) is carried out, then the contribution of the second terms will be negligible as compared to the first terms on the right-hand side of Eq. (36). As such, the ratio of these integrals provide a means to estimate the azimuth angle α.

Based on this premise, we organize the acceleration data collected at a triaxial sensor into $(N \times 1)$ arrays $\mathbf{s}_x$, $\mathbf{s}_y$, and $\mathbf{s}_z$ where N denotes the extent of the time window that contains an event of interest. Numerical integration of the array $\mathbf{s}_z$ (e.g., by using Simpson's Rule) yields the velocity array $\mathbf{v}_z$. It follows from the previous discussion that we can compute two correlation coefficients as,

$$\rho_{zx} \equiv \mathbf{v}_z \cdot \mathbf{s}_x, \quad \rho_{zy} \equiv \mathbf{v}_z \cdot \mathbf{s}_y. \tag{37}$$

The ratio of these coefficients yields the tangent of the azimuth angle of propagation direction. To wit,

$$\alpha = \tan^{-1}\left(\frac{\rho_{zx}}{\rho_{zy}}\right). \tag{38}$$

Note that, in deriving this equation, we have presumed the ideal situation where the triaxial sensor is inserted in such a way that no leakage exists between the z direction and the ground plane (i.e., all the motion in the vertical direction is due to the Rayleigh wave) and that the Rayleigh wave energy is dominant. As it will be demonstrated with experimental data in Section 6, these assumptions are quite accurate for impact-generated signals from near-field sources located in the ground plane.

4. Seismic and acoustic event detection

In the field, many events can contribute to seismic and acoustic readings. To accurately determine direction-of-arrival and locate the source of an event of interest, discriminating against other interfering sources is important. With short-range seismic and acoustic signals, we can assume high signal-to-noise-ratio, and that most of the energy contained in the signal belong to the event of interest.

For seismic event detection, time-sampled acceleration signal in x, y, and z directions are organized into column vectors as shown in Eq. (22). The simple scheme developed for event detection involves first dividing the collected record into time windows of N samples where an event can be well-contained. A sample covariance matrix is formed from zero-mean data at each window. The eigenvalues of the sample covariance matrix as a function of window number gives an indication of the signal energy contained in each window as a function of time. The magnitude of the eigenvalues of each sample covariance matrix is a good indicator of the presence of a seismic event of interest. This simple process can be performed on sliding time windows across the entire data record. Because of the lower sampling rate, a plot of the three eigenvalues as a function of time suppresses the temporal details of the raw waveforms while heightening the sensitivity to a waveform that is

coherent in all three channels. The same strategy outlined here for seismic event detection can also be applied to acoustic data to determine the presence of an acoustic event.

5. Source localization using direction-of-arrival estimates

The estimated seismic or acoustic direction-of-arrivals for a given source can be combined to obtain its location. We begin by defining the distance (ℓ_p) between an arbitrary point, $\mathbf{r} = [x, y]^{\mathrm{T}}$, in the ground plane, and the line formed by the estimated direction-of-arrival at the pth ($1 \leqslant p \leqslant P$) seismic or acoustic sensor as illustrated in Fig. 2.

The pth sensor is located at $\mathbf{r}_p = [x_p, y_p]^{\mathrm{T}}$, and the unit vector perpendicular to the estimated direction-of-arrival is $\mathbf{n}_p = [-\sin(\alpha_p), \cos(\alpha_p)]^{\mathrm{T}}$. Therefore,

$$\begin{aligned} &\ell_p(\mathbf{r}) = \mathbf{n}_p \cdot (\mathbf{r}_p - \mathbf{r}), \quad \text{or equivalently,} \\ &\ell_p(x, y) = (y_p - y)\cos(\alpha_p) - (x_p - x)\sin(\alpha_p). \end{aligned} \tag{39}$$

Then, we define the objective to be the determination of the point in the ground plane, say $\mathbf{r}^* = [x^*, y^*]^{\mathrm{T}}$, that is *closest*—with respect to some proper metric—to lines formed by the estimated direction-of-arrivals at all sensors using the ℓ_p's defined in Eq. (39). For the said purpose we first define the vector,

$$\ell(\mathbf{r}) = [\ell_1(\mathbf{r}), \ell_2(\mathbf{r}), \ldots, \ell_P(\mathbf{r})]^{\mathrm{T}} \tag{40}$$

and the weighting matrix

$$\mathbf{W}(\mathbf{r}) = \mathrm{diag}[w_1(\mathbf{r}), w_2(\mathbf{r}), \ldots, w_P(\mathbf{r})]^{\mathrm{T}} \tag{41}$$

each component of which is defined as the product of the uncertainty in the estimated direction-of-arrival (σ_p) and the distance between the sensor location ($\mathbf{r}_p$) and the point $\mathbf{r}$, i.e.,

$$w_p(\mathbf{r}) = \sigma_p \times \|\mathbf{r}_p - \mathbf{r}\|_{L_2}. \tag{42}$$

Note that, the value of each weight (w_p) is the small-angle approximation of an arc-length swept by the angle σ_p of a circle with radius $\|\mathbf{r}_p - \mathbf{r}\|_{L_2}$ centered the sensor location ($\mathbf{r}_p$). Using the inverse of the weights, we can define the weighted vector

$$\tilde{\ell}(\mathbf{r}) \equiv \mathbf{W}^{-1}\ell. \tag{43}$$

In doing so, we are essentially assigning less weight to a sensor that bears a more uncertain direction-of-arrival and to a sensor that is located further from the source. For a non-weighted source location estimation, the matrix $\mathbf{W}$ may simply be set to identity. Note that, $\mathbf{W}$ becomes singular for the pathologic case when the source is collocated with a sensor (i.e., $\mathbf{r}_p = \mathbf{r}$). However, the acceleration or sound data (hence the estimated direction-of-arrival) for such a sensor would be useless and could easily be eliminated by placing a simple

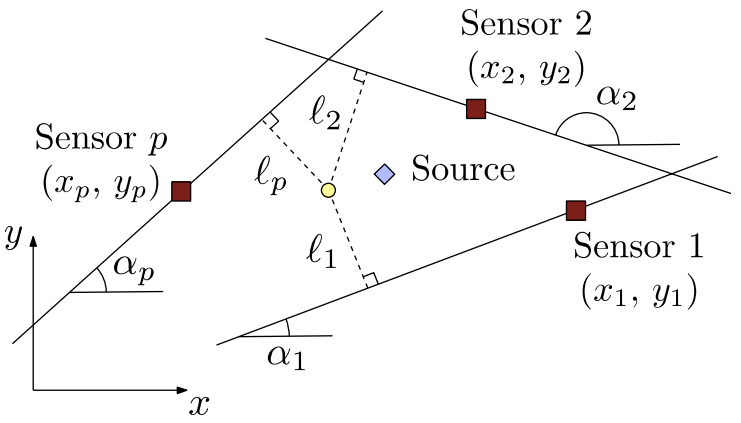

Fig. 2. Seismic source localization using DOA estimates.

threshold on the peak acceleration or the sound volume value (we could then conclude that either the source is very near the sensor p, and thus, its location will be known without direction-of-arrival estimations, or the sensor is compromised/out-of-order).

Consequently, the source location can be determined by solving the following unconstrained minimization problem:

$$\min_{\mathbf{r}} \|\tilde{\ell}(\mathbf{r})\|_{L_\alpha}, \tag{44}$$

where L_α is a properly chosen vector norm. Here, we shall consider the L_1 and L_2 norms in solving this minimization problem. Each approach has distinct advantages: the L_2 norm criterion is known to be more robust in the presence of noise (i.e., measurement errors); whereas the L_1 norm criterion is generally more robust when outliers are present (i.e., when the estimated direction-of-arrival at some sensors are highly inaccurate). The source location estimations of these two approaches are compared using experimental data in the following section.

6. Experimental studies

We have conducted a series of seismic and acoustic open-field tests at Garner Valley, California (33 40.124′ N, 116 40.376′ W), which is free of urban noise. Soils at this site are primarily soft clays, silts, and sands to 17 m, decomposed granite from 17 to 50 m, and hard granite below 50 m. Water table varies seasonally from 0 (surface) to 4 m depth. Although no specific measurement were taken, we expect that the water table was nearly at its lowest during the time of testing (month of August). As displayed in Fig. 3, six seismic sensors (accelerometers) were placed with approximately 15.24 m (50 ft) separation in a rectangular array on the ground level, and two acoustic arrays were placed near the center points of the upper-right and lower-left quadrants of the 30.48 m × 30.48 m testing grid.

Each accelerometer was a triaxial, force-balanced Kinemetrics Episensor. The seismic data was acquired, digitized, GPS time-stamped, and relayed (via wireless telemetry) to a mobile data recording station using Kinemetrics Quanterra Q330 data-loggers (for further information about this equipment, see Ref. [10]). Each acoustic array consisted of four omni-directional Behringer XM2000S microphones. These microphones were held in place at the top vertices of a simple (1.0 m × 1.0 m × 0.5 m) scaffold made of PVC pipes. The acoustic data collected by the eight microphones were acquired and time-synchronized with a Presonus

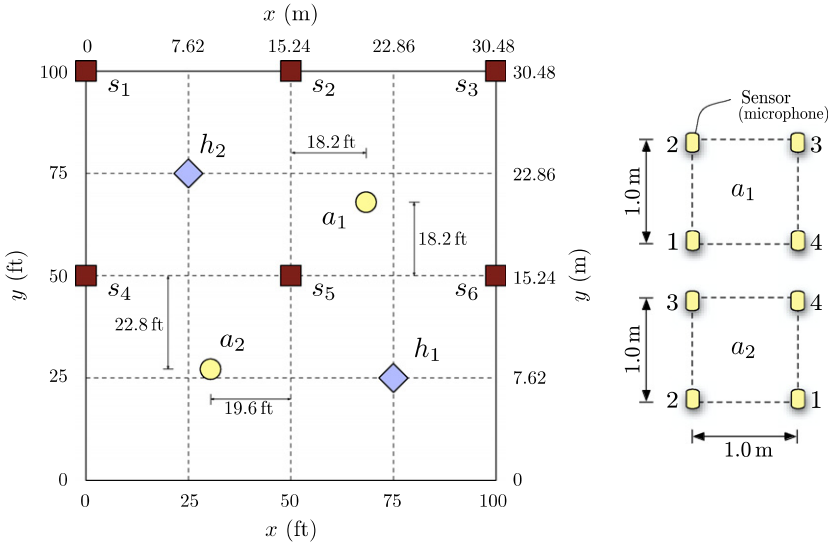

Fig. 3. Set up for the "hammering experiment." Acoustic arrays are labelled as a_1, and a_2; triaxial seismic sensors are labelled as s_1–s_6; and the (hammer) sources are labelled as h_1, and h_2. The individual sensors of the two acoustic arrays are shown on the right.

Firepod (8-channel microphone/pre-amp) recording system, and were relayed to a PC. The seismic and acoustic data were sampled at 200 Hz and 44.1 kHz rates, respectively.

Source signals were generated by striking a heavy metal plate with a hammer at two distinct locations, as illustrated Fig. 3. Because they were produced by an impact, the acoustic and the seismic source signals were both wideband. In Experiments I and II, the sources (labelled as h_1, and h_2 in Fig. 3) were located outside and inside the perimeter of the seismic array, respectively. For each experiment, a series of six vertical strikes (in approximately two second intervals) were made. An example of the recorded signals is shown in Fig. 4.

6.1. Event detection studies

In this section, we demonstrate the event detection algorithm previously described in Section 4. Event detection algorithms are necessary for automatic processing of collected data. In the absence of an automatic event detection algorithm, the analyst has to make a judgment on the location of an event, and the size of the window of time-domain data to be processed by the localization algorithms.

The applications of the event detection algorithm to acoustic and seismic time-domain data are similar; and here, we demonstrate it for seismic data collected at sensor 1 during Experiment I. In the present study, we used sliding windows of $N = 50$ samples with 25 samples overlapping between successive windows. Fig. 5 shows the plot of eigenvalues of the sample covariance matrices as a function of window number. It is evident from this figure that the six significant hammer strikes in the data are contained in windows where λ_3 are above 10^{-4}. Data from these windows are used to estimate source direction-of-arrival's via seismic (covariance matrix analysis, surface Fourier transform) and acoustic (approximate maximum likelihood) localization algorithms.

6.2. Acoustic direction-of-arrival results

The acoustic signals from the six hammer strikes are wideband, and thus, their spectra are non-uniform. Therefore, the previously mentioned enhancements to the basic AML method, namely frequency-bin weighting and channel whitening, must be employed.

The strike signals were identified using the previously outlined event detection algorithm. The channel whitening operation is performed on these detected strike signals using the noise power spectrum collected during the quiet periods (in the absence of hammering). For example, Figs. 6 and 7 display, respectively, the

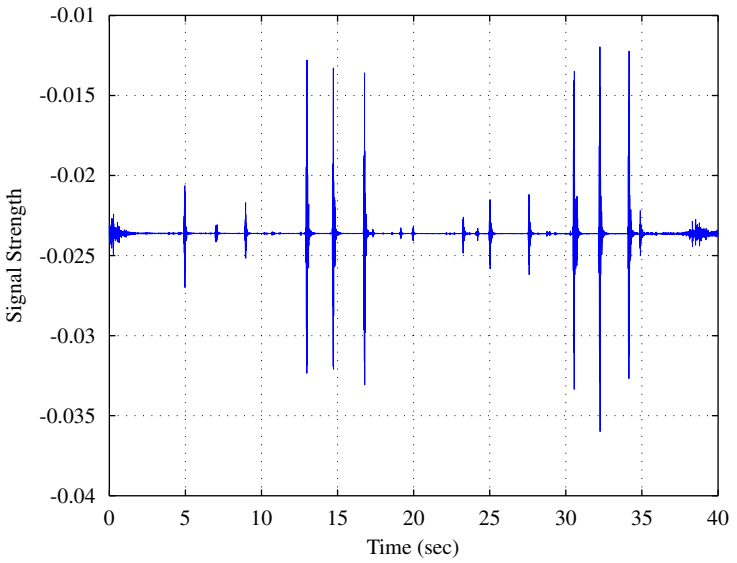

Fig. 4. Vertical component of the seismic (hammer strike) signal recorded at sensor 1 during experiment I.

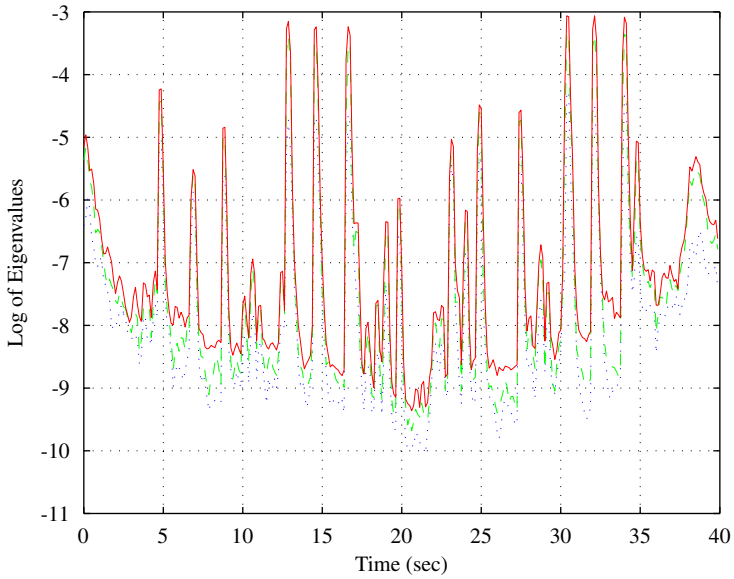

Fig. 5. Eigenvalues ($\lambda_1 > \lambda_2 > \lambda_3$) of the sliding sample covariance matrices as a function of time for data collected at seismic sensor 1 during Experiment I (λ_1, λ_2, and λ_3 are marked with solid, dashed, and dotted lines, respectively).

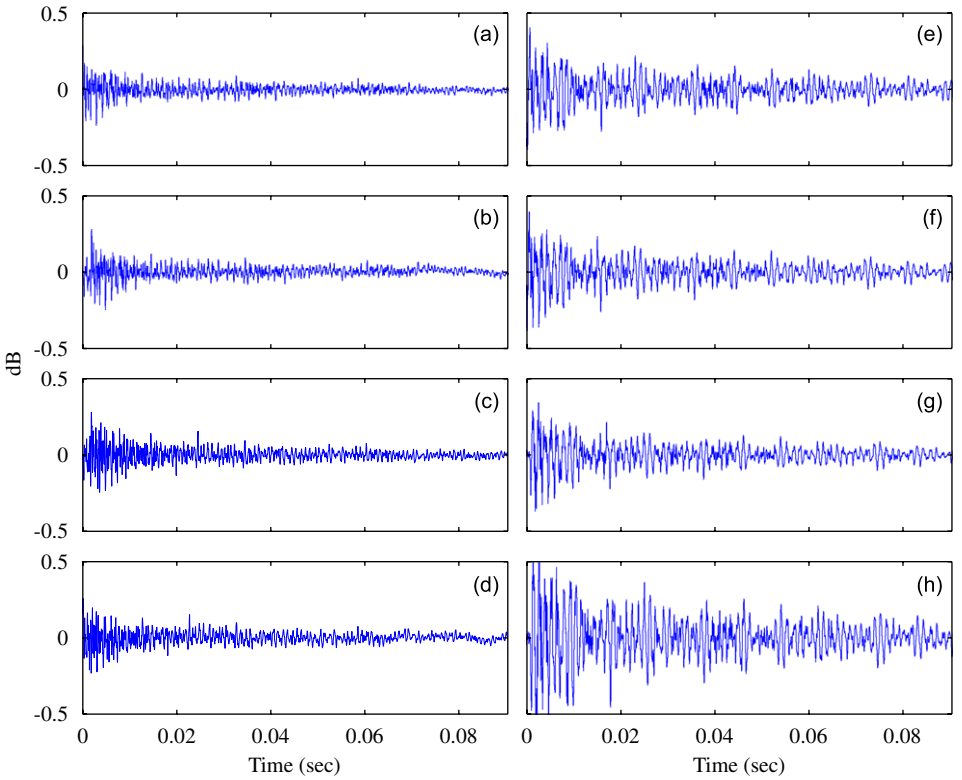

Fig. 6. Time domain acoustic waveforms for Experiment I strike 3 at Array 1's Sensors 1, 2, 3, 4 (a, b, c, d), and at Array 2's Sensors 1, 2, 3, 4 (e, f, g, h).

time and frequency domain data collected at the two acoustic array for Experiment I, strike 3. Fig. 8 displays the power spectral density of the recorded background noise for both arrays, and the spectra of the whitened signals are given in Fig. 9. As expected, the power spectral density of the received strike signal after whitening

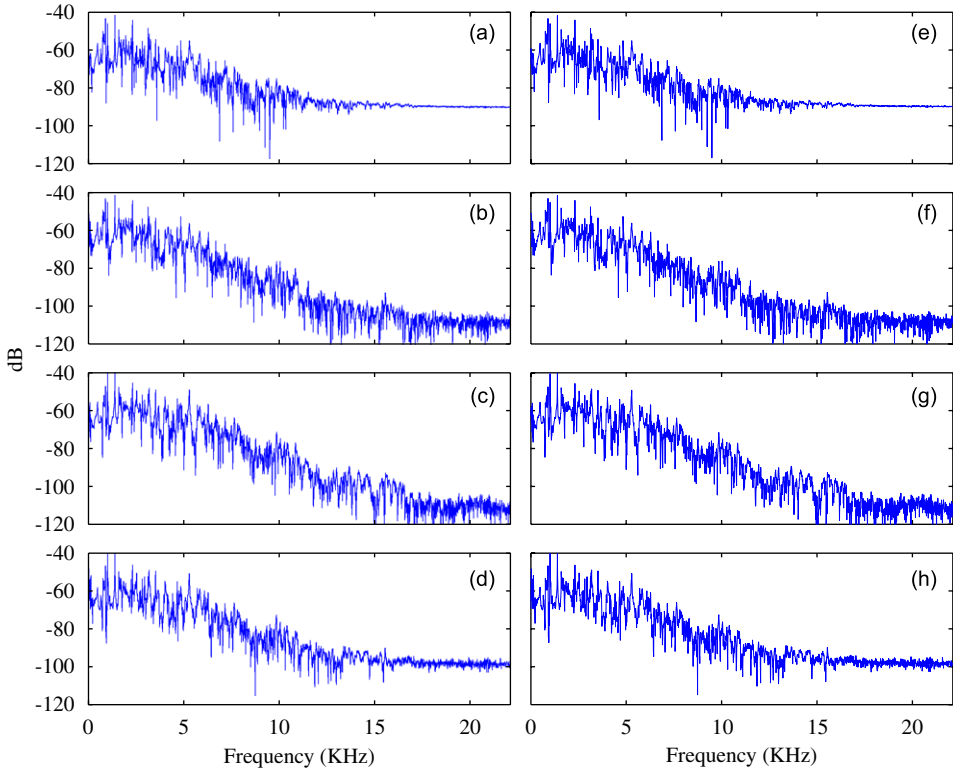

Fig. 7. Power spectrum of the received acoustic signal for Experiment I strike 3 at Array 1's Sensors 1, 2, 3, 4 (a, b, c, d), and at Array 2's Sensors 1, 2, 3, 4 (e, f, g, h).

is more uniform than it was before whitening. We observed the same for all other strikes including those in Experiment II. The whitened signals were processed through the approximate maximum likelihood algorithms enhanced with frequency-bin weighting to estimate the source locations for both experiments. As there are only two acoustic arrays, the AML algorithm yields a single direction-of-arrival estimation for each array. Therefore, the source location estimation from direction-of-arrival data is trivial (the source location simply lies at the intersection of the two direction-of-arrival estimates), and the least-squares procedure mentioned in Section 5 becomes unnecessary.

The utility of the channel whitening and frequency-bin weighting enhancements are illustrated by the source location estimates for Experiment I strike 3 provided in Table 1. As these results indicate, the approximate maximum likelihood algorithm enhanced with channel whitening *and* frequency-bin weighting yields the best estimates. The same is true for all other strikes, including those for Experiment II (these results are omitted for brevity).

The source location estimates and their absolute errors for all strikes are given in Table 2. As these results indicate, several strikes yielded source location estimates with quite large absolute errors, such as strikes 4 and 6 in Experiment I, and strike 6 in Experiment II. The effect of these outliers can be diminished if the median of estimations for successive strikes are used instead of their average value. This approach is quite feasible in practical situations were a target/source is stationary. For moving targets, which are out of the scope of the present investigation, a more sophisticated procedure may be necessary.

6.3. Seismic direction-of-arrival estimation via covariance matrix analysis

Results of the direction-of-arrival estimation via covariance matrix analysis for both experiments (I and II) are plotted in Fig. 10, and tabulated in Table 3. Again, σ_p denotes the variance in the estimated direction-of-arrival at sensor p. Since there were six hammer strikes performed at the same location, the algorithm

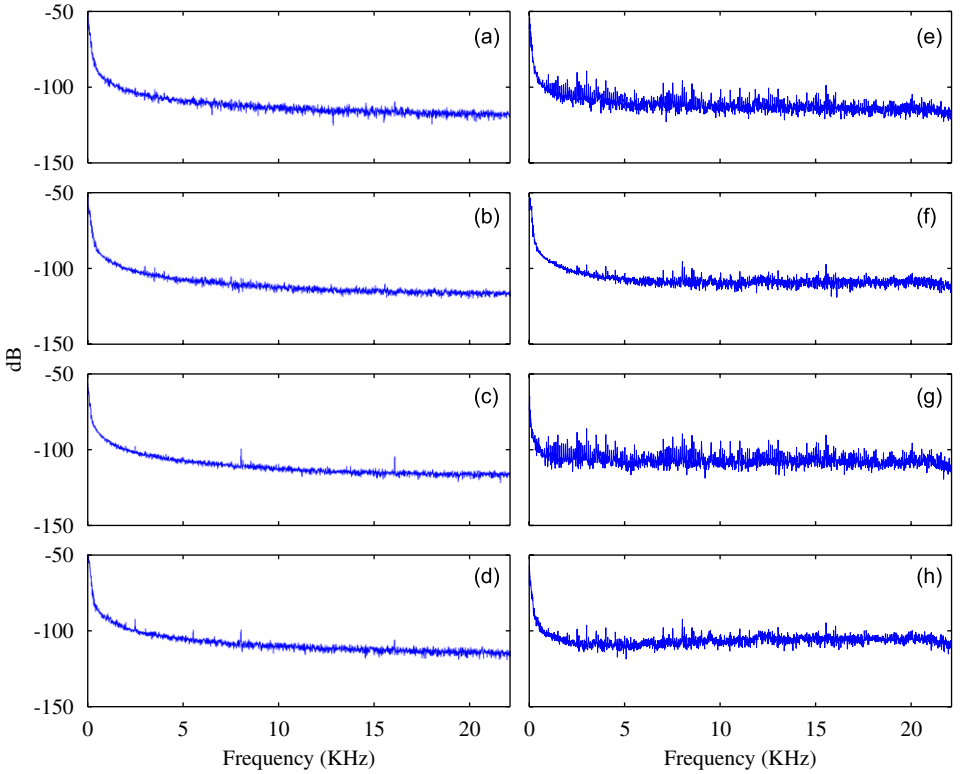

Fig. 8. Power spectrum of the received acoustic noise for Experiment I at Array 1's Sensors 1, 2, 3, 4 (a, b, c, d), and at Array 2's Sensors 1, 2, 3, 4 (e, f, g, h).

estimates six direction-of-arrivals (i.e., one for each strike). The final estimated direction-of-arrival at sensor p is the average of these six estimated direction-of-arrivals. The variance of these six estimates is σ_p.

Note that the directions defined with the covariance matrix analysis have a 180^o ambiguity. The directions found at sensor 1 in Experiment I and at sensor 3 in Experiment II appears to be orthogonal to the directions of the two sources. Therefore, it is reasonable to conclude that the data collected at these sensors have more energy belonging to the Love wave than the Rayleigh wave. As such, the directions picked by these sensors are due to Love waves, which is perpendicular to the propagation direction. In addition to the 180^o ambiguity, this is an apparent weakness of the covariance matrix analysis approach.

6.4. Seismic direction-of-arrival estimation via surface wave analysis

Results of the direction-of-arrival estimation via SWA for both experiments (I and II) are plotted in Fig. 11, and tabulated in Table 4. Unlike what is observed via covariance matrix analysis, we can see that directions found at *all* sensors are pointed approximately in the direction of the source. We also observe that the direction-of-arrival's in Experiment II are more accurate than those in Experiment I with less variation between events. This may be due to the fact that the source is closer to the sensors in Experiment II, and hence the collected data have larger signal-to-noise-ratio.

6.5. Seismic source localization results

Using the seismic direction-of-arrival estimations provided in Sections 6.3 and 6.4, we performed both weighted and un-weighted L_2 and L_1 optimizations to obtain source locations for the two experiments. Tabulated in Table 5, these results indicate that the weighted versions of both L_2 and L_1 norm criteria performed better than their un-weighted counterparts in all cases for direction-of-arrivals obtained from both

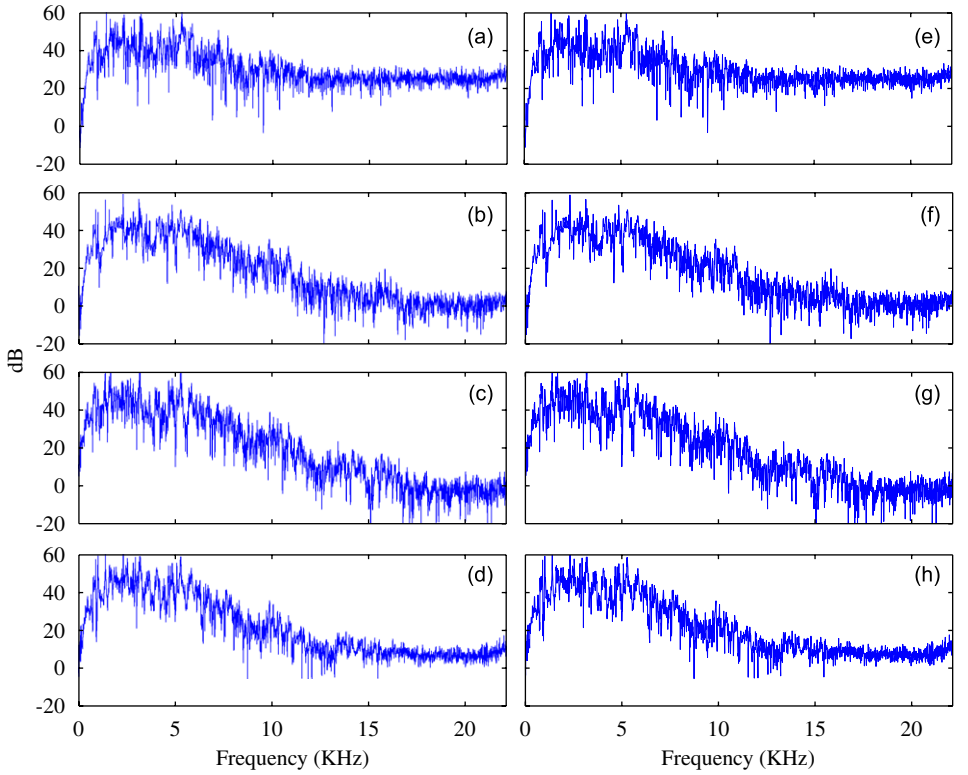

Fig. 9. Power spectrum of the received acoustic signal for Experiment I strike 3 after whitening at Array 1's Sensors 1, 2, 3, 4 (a, b, c, d), and at Array 2's Sensors 1, 2, 3, 4 (e, f, g, h).

Table 1
Estimated source coordinates (m) via the enhanced AML algorithm using acoustic data (CW: channel whitening, FBW: frequency bin weighting)

Exp., strike	True coord.	Est. (x, y), and [abs. error] per AML enhancement			
	(x, y)	None	CW	FBW	CW + FBW
I, 3	(22.9, 7.6)	(35.8, 15.8) [15.3]	(30.9, 13.3) [9.8]	(12.4, 4.6) [10.9]	(23.9, 7.3) [1.1]
II, 5	(7.6, 22.9)	(13.3, 36.7) [15.0]	(9.2, 34.4) [11.6]	(7.0, 16.2) [6.7]	(7.1, 24.3) [1.5]

Table 2
Source coordinate estimates and their absolute errors (m) obtained using acoustic AML method

Exp., coord.	Strike number						Avg.	Med.	True	σ
	{1	2	3	4	5	6}				
I, x	24.5	24.2	23.9	16.2	21.2	18.6	21.4	22.5	22.9	3.4
I, y	6.9	6.0	7.3	21.4	9.6	15.6	11.1	8.4	7.6	6.1
I, err.	1.8	2.1	1.1	15.3	2.6	9.1	3.8	0.9*	0.0	5.7
II, x	7.2	7.8	10.6	9.4	7.1	13.7	9.3	8.6	7.6	2.5
II, y	20.7	26.0	22.1	22.7	24.3	14.0	21.6	22.4	22.9	4.2
II, err.	2.2	3.1	3.1	1.8	1.5	10.8	2.1	1.1*	0.0	3.5

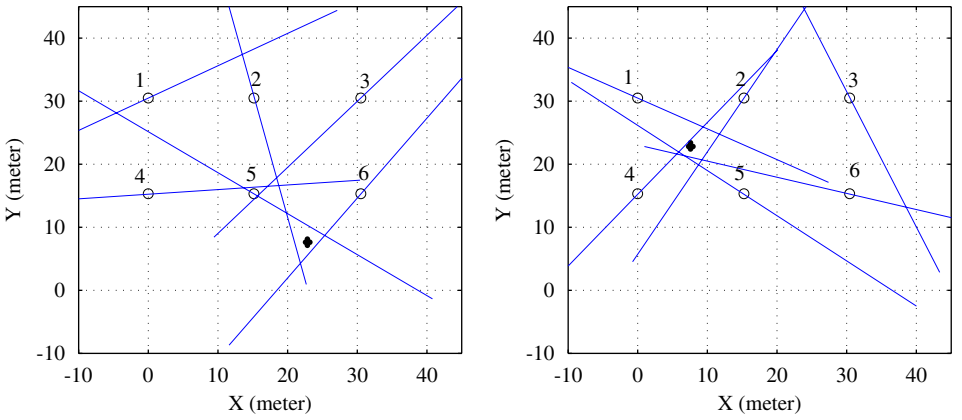

Fig. 10. Average DOA estimation results from covariance matrix analysis for experiments I (left) and II (right). Circles and solid diamonds represent seismic sensor and the true source locations, respectively; the lines represent DOA estimates (α_p) at each sensor.

Table 3
Azimuth angles (deg.) obtained using CMA method

Exp., sensor	Strike number						Avg.	σ_p
	{1	2	3	4	5	6}		
I, s_1	−87	80	69	−47	79	69	27.2	74.36
I, s_2	−68	−74	−78	−67	−82	−86	−75.9	7.51
I, s_3	25	29	59	44	56	64	46.3	16.23
I, s_4	3.1	5.0	4.2	−1.9	4.9	9.8	4.18	3.76
I, s_5	−35	−34	−31	−40	−30	−28	−33.0	4.29
I, s_6	52	52	52	48	53	53	51.7	1.71
II, s_1	−23	−27	−26	−26	−26	−27	−26.0	1.33
II, s_2	57	57	60	59	58	59	58.4	1.02
II, s_3	−77	−80	−63	−61	−42	−68	−65.0	13.8
II, s_4	48	48	49	49	49	49	48.71	0.39
II, s_5	−30	−35	−36	−40	−37	−37	−35.6	3.31
II, s_6	−11	−16	−16	−14	−18	−11	−14.4	2.80

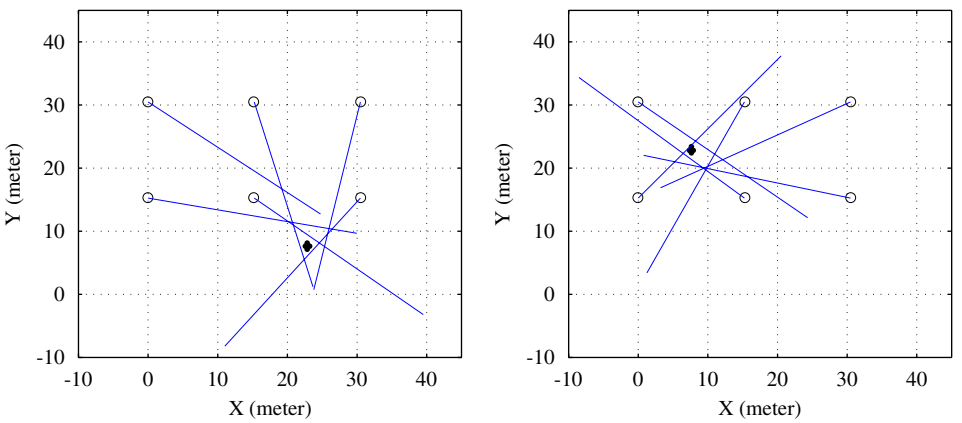

Fig. 11. Average DOA estimation results from Surface Wave Analysis for experiments I (left) and II (right). Circles and solid diamonds represent seismic sensor and the true source locations, respectively; the lines represent DOA estimates (α_p) at each sensor.

Table 4
Azimuth angles (deg.) obtained using SWA method

Exp., sensor	Strike number						Avg.	σ_p
	{1	2	3	4	5	6}		
I, s_1	−36	−35	−35	−40	−34	−34	−35.7	2.23
I, s_2	−68	−71	−80	−67	−78	−80	−74.0	5.99
I, s_3	−105	−105	−100	−110	−97	−99	−102.7	4.82
I, s_4	−5	−6	−15	−10	−11	−15	−10.5	4.36
I, s_5	−34	−37	−42	−36	−36	−38	−37.3	2.66
I, s_6	−131	−130	−130	−132	−128	−128	−129.7	1.66
II, s_1	−38	−39	−37	−38	−36	−35	−37.0	1.48
II, s_2	−119	−119	−116	−116	−118	−115	−117.3	1.49
II, s_3	−153	−154	−151	−157	−156	−149	−153.5	3.17
II, s_4	47	48	48	48	48	48	47.7	0.38
II, s_5	142	142	141	141	140	142	141.2	0.88
II, s_6	165	167	168	168	167	169	167.1	1.47

Table 5
Seismic source localization results (m) using different least-squares criteria

Exp., method	True coord.	Est. (x, y), and [abs. error] per least-squares criteria			
	(x^*, y^*)	L_2	Wt. L_2	L_1	Wt. L_1
I, CMA	(22.9, 7.6)	(18.0, 19.6) [13.0]	(26.0, 9.7) [3.7]	(18.7, 16.6) [9.9]	(25.3, 8.7) [2.6]
I, SWA	(22.9, 7.6)	(24.5, 9.8) [2.7]	(24.8, 8.4) [2.1]	(26.0, 10.4) [4.2]	(24.6, 8.1) [1.8]*
II, CMA	(7.6, 22.9)	(16.0, 24.3) [8.5]	(9.4, 24.8) [2.6]	(11.7, 24.8) [4.5]	(9.5, 25.9) [3.6]
II, SWA	(7.6, 22.9)	(9.1, 21.2) [2.3]	(8.4, 23.6) [1.1]*	(9.5, 20.0) [3.5]	(8.2, 24.3) [1.5]

the covariance matrix analysis and surface wave analysis. Weighting appears to have significantly improved the source localization results using direction-of-arrivals from covariance matrix analysis. For both covariance matrix analysis and surface wave analysis, the weighted L_1 norm performed better in Experiment I where the estimated direction-of-arrivals had larger variances; while the weighted L_2 norm performed better in Experiment II where the estimated direction-of-arrivals were more reliable. These observed behaviors are in line with the known features of the L_1 and L_2 criteria.

6.6. A basic fusion of acoustic and seismic localization results

Simultaneous use of acoustic and seismic sensor arrays for source localization has several potential benefits. To wit, seismic and acoustic signals are propagated through different media (air and ground), therefore they are not necessarily vulnerable to identical complications. This potentially enhances the robustness of estimations. For example, acoustic arrays and the source may not have a direct line-of-sight, and intervening objects or nearby reflective surfaces (causing echoes) may lead to inaccurate location estimates through the use of acoustic data. Additionally, weather conditions (such as intense wind) may severely reduce the signal-to-noise-ratio in acoustic data. Seismic arrays are generally insensitive to such mishaps. Conversely, the source may not impart sufficient energy into the ground while at the same time it may be audible (such as an idling stationary terrestrial vehicle, a low-flying aerial vehicle, or a fired hand-held weapon). Whatever the combinations of such circumstances are, an analyst may still be capable of making accurate, albeit *ad hoc*,

estimations of the source location if she/he is provided with all available results from acoustic and seismic arrays. Furthermore, if *both* acoustic and seismic results are reliable, they can be combined/fused statistically to increase the accuracy of location estimates. While an advanced study of fusion is out of the scope of the present study, we shall make a very basic attempt here.

We have noted that surface wave analysis approach is generally superior to covariance matrix analysis for seismic source localization. So, we shall use the direction-of-arrival estimations via surface wave analysis for fusion. Furthermore, we have noted that when the source location is outside the perimeter of the seismic array (as in Experiment I), the weighted L_1 criterion is superior to the weighted L_2 criterion, while the converse is true when the source location is inside the perimeter of the seismic array (as in Experiment II). Armed with these, we shall use the surface wave analysis results processed with weighted L_1 and L_2 criteria for Experiments I and II, respectively, for fusion (these particular results were marked with an asterisk symbol in Table 5). The utility of the aforementioned weighting schemes is the reduction of the influence of outliers. For acoustic signals, the influence of the outliers can be reduced by using the median rather than the average estimations (as there were only two acoustic arrays and the least-squares procedures could not be used). Therefore, we shall use the median acoustic approximate maximum likelihood results (these particular results were marked with an asterisk symbol in Table 2).

These "best" estimations are reproduced in Table 6 along with a simple average of their values. An inspection of the average (fused) results indicates that the absolute estimation error for Experiments I and II are 0.85 and 0.95 m, respectively. These final results are more accurate than the best estimates of both the surface wave analysis and the enhanced approximate maximum likelihood methods. Given the potential inaccuracies in field measurements and inappropriate sensor placement/alignment, the fused results are remarkably accurate. On a final note, an alternative approach for fusion would have been to use the acoustic and seismic DOA results in a combined least-squares estimation. We defer this study and consideration of other, more advanced, approaches for data fusion to a subsequent study.

7. Summary and conclusions

We have described several methods for localization of acoustic and seismic wideband sources. For acoustic source localization, we have enhanced an approximate maximum-likelihood method, originally devised for narrowband and relatively wideband sources, via frequency bin weighting and channel whitening operations. For seismic sources, we have considered an existing method, dubbed covariance matrix analysis that was originally devised for long-range detection and localization, and a new method, which we named surface wave analysis surface wave analysis. Each of the aforementioned methods yields the direction-of-arrival of the source signals. We have devised several weighted least-squares methods that combine the direction-of-arrival estimates and yield the source location.

Using experimental data, we have compared the performance of the original and the enhanced approximate maximum likelihood algorithms, of the covariance matrix analysis and surface wave analysis algorithms, and of the various weighted least-squares schemes. The results indicated that the enhanced approximate maximum likelihood and the surface wave analysis algorithms, which were developed in the present study, are more accurate than the basic (original) approximate maximum likelihood and the covariance matrix analysis algorithms, respectively. Further, we have observed that the weighted L_1 and the weighted L_2 norm criteria—which are used for obtaining source location estimations from direction-of-arrival estimations—yield better results when the source was placed outside and inside of the sensor array perimeter, respectively. We have also

Table 6
Best seismic and acoustic source localization results and their average

Exp.	True coords.	Localization method		Average
	(x, y)	Seismic	Acoustic	
I	(22.9, 7.6)	(24.6, 8.1)	(22.5, 8.4)	(23.5, 8.2)
II	(7.6, 22.9)	(8.4, 23.6)	(8.6, 22.4)	(8.5, 23.0)

attempted a basic fusion of acoustic and seismic source localization results to improve the accuracy of estimations. Fused results had less than 1 m of absolute estimation error for all of the (two) experiments performed; and the accuracy afforded by fusion was better than those of the individual acoustic and seismic methods.

We note here that the computer implementation of the presented algorithms have not been optimized for speed. Nevertheless, it takes only a few seconds to carry out the processing of Eq. (14) using a laptop with a 1.6 GHz processor. A similar time is required for seismic localization via, for example, the processing of Eqs. (38) and (44). Therefore, it appears that these methods are ultimately amenable for near real-time localization.

Experiments—other than those presented in this study—involving moving vehicles and human footsteps were also conducted. However, an investigation of these experiments are deferred to a sequel, as the processing of such data is likely to require new algorithms, or extensions/enhancements of those presented in this study.

Acknowledgments

The authors gratefully acknowledge that this research was supported, in part, by the National Science Foundation (NSF) under award number EF-0410438, by NSF Science and Technology Center for Embedded Network Sensing (CENS) under cooperative agreement CCR-0121778, by AROD-MURI PSU contract 50126, and by the UC-Discovery grant co-sponsored by the ST Microelectronics Corporation. The authors would also like to thank Professor John Wallace for providing the nees@UCLA equipment (accelerometers and data acquisition systems), Dr. Daniel Whang, Steve Kang, Andreas Ali, and Chiao-En Chen for their participation in the experiments, and Professor R. Kirlin for sharing various documents and subroutines. The results, opinions, and conclusions expressed in this paper are solely those of the authors and do not necessarily represent those of the sponsors.

References

[1] E.M. Carapezza (Ed.), Unattended ground sensor technologies and applications IV, *Proceedings of SPIE* 4743 (2002).
[2] J. Chen, R. Hudson, K. Yao, Maximum-likelihood source localization and unknown sensor location estimation for wideband signals in the near-field, *IEEE Transactions on Signal Processing* 50 (2002) 1843–1854.
[3] J. Chen, K. Yao, R. Hudson, Source localization and beamforming, *IEEE Signal Processing Magazine* 19 (2002) 30–39.
[4] J. Chen, L. Yip, J. Elson, H. Wang, D. Maniezzo, R. Hudson, K. Yao, D. Estrin, Coherent acoustic array processing and localization on wireless sensor network, *Proceedings of the IEEE* 91 (2003) 1154–1162.
[5] E. Flinn, Signal analysis using rectilinearity and direction of particle motion, *Proceedings of the IEEE* 53 (12) (1965) 1874–1876.
[6] R.L. Kirlin, W.J. Done (Eds.), *Covariance Analysis for Seismic Signal Processing, Geophysical Development Series*, Vol. 8, Society of Exploration Geophysicists, Tulsa, Oklahoma, 1998.
[7] G.M. Jackson, I.M. Mason, S.A. Greenhalgh, Single-station triaxial data analysis, in: R.L. Kirlin, W.J. Done (Eds.), *Covariance Analysis for Seismic Signal Processing, Geophysical Development Series*, Vol. 8, Society of Exploration Geophysicists, Tulsa, Oklahoma, 1998, pp. 275–289.
[8] N. Magotra, N. Ahmed, E. Chael, Single-station seismic event detection and location, *IEEE Transactions on Geoscience and Remote Sensing* 27 (1989) 15–23.
[9] N. Magotra, N. Ahmed, E. Chael, A comparison of two parameter estimation schemes, *Proceedings of the IEEE* 74 (5) (1986) 760–761.
[10] G.E. Brown, Jr., *Network for Earthquake Engineering Simulation* (*NEES*), University of California, Los Angels, ⟨http://www.nees.ucla.edu⟩.
[11] L. Yip, J. Chen, R. Hudson, K. Yao, Numerical implementation of the AML algorithm for wideband DOA estimation, *Proceedings of SPIE* 5205 (2003) 164–172.
[12] H. Wang, C.E. Chen, A. Ali, S. Asgari, R.E. Hudson, K. Yao, D. Estrin, C. Taylor, Acoustic sensor networks for woodpecker localization, *Proceedings of SPIE* 5910 (2005) 1–12.